FSI simulation of flexible tandem insect wings in counter stroke

Y.H. CHEN and M. SKOTE
School of Mechanical and Aerospace Engineering
Nanyang Technological University
50 Nanyang Avenue, Singapore 639798
SINGAPORE

C. STEFFEN and H. NORDBORG
Institute for Energy Technology
HSR University of Applied Sciences
Rapperswil
SWITZERLAND
mskote@ntu.edu.sg http://www3.ntu.edu.sg/home/mskote/

Abstract: - Bionic micro-air vehicles (MAV) having the maneuverability of dragonflies would be capable of fast forward flight, hovering and even backward flight. In order to achieve desirable designs for high performing MAVs, it is essential to understand the aerodynamics and structures of the insect wings and more importantly, the interactions between the operating flows and flexible structural wings. Here, we present a fluid-structure interaction model which integrates the realistic structural flexibility of the dragonfly wings with the actual counter-stroke flapping trajectories. Hence, we are able to study the aero-elastic deformation and aerodynamic forces acting on the flapping wings, in the hope that future MAV designs would perform closer to the agile natural fliers. Verification of the simulation framework is performed by a number of rigorous tests with comparison to past experiments and simulations.

Key-Words: dragonfly wings, flapping flight, tandem wings, counter stroke, CFD, CSM, FSI

1 Introduction

Among the nature flyers, insects have gained the attention and interests of researchers owing to their compact size, maneuverability and agility. Bionic Micro-Air Vehicles (MAVs) mimicking the flapping insects have numerous applications in fields as military reconnaissance. Such application requires MAVs with high maneuverability. Within all the flapping insects, dragonflies in particular fly in a highly maneuverable manner. They are capable of developing fast forward flight, hovering and even backward flight. Moreover, dragonflies operate each of their wings independently, maintaining a specific phase relation between the wing pairs [1-3]. At least three distinct flight styles are recognized in dragonflies: out-of-phase or counter stroking, in-phase or parallel stroking, and gliding [4].

There have been many attempt to use computational fluid dynamic (CFD) models replicating the idealised flapping motion of hovering flights, intending to reveal the insight of unsteady aerodynamic force generation process, but only three-dimensional (3-D) rigid flat planes are modelled [5, 6].

Only a few research groups have considered the flexibility of the wing and its interaction with the fluid in their 3-D CFD simulations. Smith and co-workers implemented the unsteady aerodynamic panel method in simulating the flight of the hawk-moth *Manduca sexta* [7-9]. They first forcibly simulate the wing twist and root angular motion of a rigid wing model, and adopted potential flow model to compute the aerodynamic forces acting on the wing. They then transfer the aerodynamic loads into a structural wing model build with the finite element method (FEM) to obtain the wing deformation. Their simulation approach is much more promising if detailed in-flight kinematic data and actual morphological and material properties of the flapping wing is integrated. The main limitations in their study are that the wing model was simplified so that the leading edge effect was ignored and the 3-D wing profile was not included; the FEM wing model was not modelled according to the actual material properties of the membrane and vein but as a linear elastic structure; and no actual in-flight trajectory was implemented in the simulation. Ho et al. [48] considered the flexibility of the wing, and

built a structural and CFD model with integrated framework and membranes. Even the arrangement of the spars mimics the actual veins. However, the 3-D surface profile such as the corrugation as well as the actual flapping trajectory of the wing was left aside. With the 3-D corrugation, the camber of the wing and the aerodynamic forces acting will be much different, and the simulation results will be much closer to the actual flight situation. In the computational model of [48], the motion of the leading edge and chord were prescribed as one sinusoidal motion of time. However, from our kinematic studies [15] it is shown that the leading edge and trailing edge demonstrates different periodic motions. Thus, in our fluid-structure interaction (FSI) model, different kinematic models will be used to prescribe the motions of the leading edge and trailing edge respectively to illustrate both the motion and deformation of the wing during flapping.

So far there are a few attempts in cooperating in-flight wing kinematics into 3-D CFD model of an insect with deforming wings was published recently [10]. More than one hundred natural features and pre-marked points on the flying insect wings were tracked by four high-speed cameras, and then used to reconstruct the deforming surface topography of the wings [10-13]. Commercial software Gambit 2.4.6 and Fluent 6.2.16 were used by [10] to create the geometry, create the mesh and analyze the aerodynamic effects on the deforming wings. The time-dependent wing motion and deformation were incorporated into the solver through the dynamic mesh feature by a user-defined-function (UDF). Although in-flight wing kinematics and deformation are both considered, only the aerodynamic effects on the wing were analyzed, the aero-elastic interaction between the deformable wing and the fluid is lacking.

Aero-elasticity involves not just the external aerodynamic loads and the way they change but also the structural, damping and mass characteristics of the structure. It is the study of the mutual interaction that takes place within the triangle of the inertial, elastic, and aerodynamic forces acting on structural members exposed to an air-stream. Since a dragonfly wing is not rigid and controlled only from wing root, the aerodynamic forces acting on the flapping wing bound to induce certain deformation on the wing which in turn alters the aerodynamic loads. Thus, to acquire a better insight of dragonfly flights, aerodynamic effects on the deforming wing along is not enough; the mutual interaction between the fluid and the structure should be taken into account.

Hence, our research aims to build FSI model which integrates the 3-D structural characteristics and the flexibility of the wing with the actual flapping trajectories, so that both the structural and aero-elastic deformation and aerodynamic forces acting on the flapping wings can be dissected.

2 Methodology

In the present FSI study, ANSYS Fluent, ANSYS Mechanical and the System Coupling packages from ANSYS Workbench 16.2 was used in creating the wing model, meshing, and two-way coupling of the computational fluid dynamic (CFD) solver and the finite element method (FEM) based computational structure mechanics (CSM) solver.

In the following sections, the present FSI modelling of the tandem dragonfly wings is presented with the geometric and kinematic modelling in Sec. 2.1, the setup of the CFD modelling in Sec. 2.2 and the implementation of material properties to the structural wing model in Sec. 2.3.

2.1 Geometric and kinematic modelling of the dragonfly wings

In the present FSI modelling, the fore- and hind-wings were modelled tandemly, with a uniform thickness of 0.13 mm, which adopts the maximum thickness of the leading edge spar measured [14]. As shown in Fig. 1(a), the planform of the model wings was traced from the fore- and hind-wings of the dragonfly *Sympetrum flaveolum*, which is the species closest to *Sympetrum sanguineum* [4] available locally. The wings were then scaled accordingly with a forewing length of 26.38 mm [4], from the same individual whose kinematics was used in the present simulations. The fore- and hind-wing models have a mean chord length of 5.54 mm and 7.45 mm, and a planform area of 146.3 mm^2 and 190.0 mm^2, with an aspect ratio of 9.52 and 6.84, respectively.

The flapping kinematics used in the present simulation was adapted from the experimental data acquired by Wakeling and Ellington [4] and Chen et al. [15]. In accordance to the kinematic experiments, the dragonfly body was inclined at an angle χ to the horizontal X-axis, as seen in Fig. 1(b), and the stroke planes were inclined to the horizon at the stroke plane angles β_f and β_h for the fore- and hind-wing respectively. For clearer illustration of terms defined, only the stroke plane of the hindwing is shown in Fig. 1(b). The terms are defined in a

similar manner for the forewing with the subscript 'f' instead of 'h' of the hindwing.

Moreover, the instantaneous wing position and attitude are described by the position angle ϕ, the elevation angle θ and the angle of attack α with respect to the stroke plane as shown in Fig. 1(b). The local wing-fixed coordinate system has its origin at the wing root, and the yw-axis is defined based on the rotation axis of the pitching motion lying behind the leading edge, connecting the wing root and wing tip.

In the present FSI simulations, the wing tip trajectories of the fore- and hind-wing were adapted from the free flight experiments done by Wakeling and Ellington [4]. The fitted results from the Fourier series analysis of the kinematic data [4] were used to describe the kinematic model and applied to the wing model at the wing root in the present FSI simulation. As data of the angle of attack was not available from Wakeling and Ellington's experiments, we used kinematic measurements from Chen and co-workers [15, 16] based on a similar dragonfly.

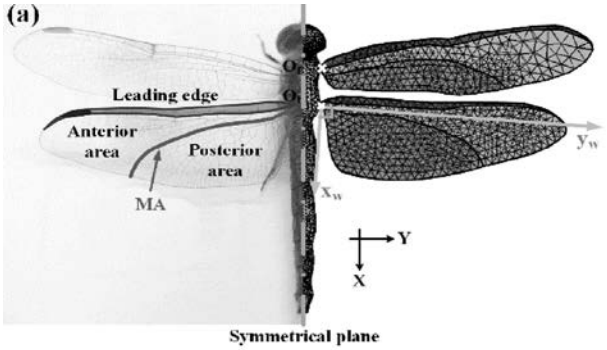

Figure 1(a). Top view showing the planform of the modelled dragonfly wings and their real counterparts. Of and Oh denote the wing root position of the fore- and hind-wing respectively. The wing roots are 2 mm away from the symmetrical plane which lies at the mid-line of the insect thorax. The structural wing consists of three regions: Leading edge, Anterior and Posterior areas, where the main area behind the leading edge is divided by the anterior median vein (MA) into anterior and posterior areas.

As shown in Fig. 1(b)(i), due to the difficulty in physically measuring the downwash related deflection of the free stream, the geometric rather than aerodynamic angles of attack are used in the present simulation, which is the geometric angle of attack α at 60% wing length with respect to the free-stream velocity in the X-direction. Similar to the wing tip trajectories, the measured angles of attack α [15] were fitted with the first five terms of the Fourier series and used as kinematic modelling in the present simulation. The flapping motions were carried out in the present simulation as three basic rotations about the local wing-fixed axis: firstly, rotation (flapping) of the wing with the positional angle ϕ about the x_w-axis; secondly, rotation (heaving) of the wing with the elevation angle θ about the z_w-axis; and lastly rotation (pitching) of the wing with the angle of attack α about the y_w-axis.

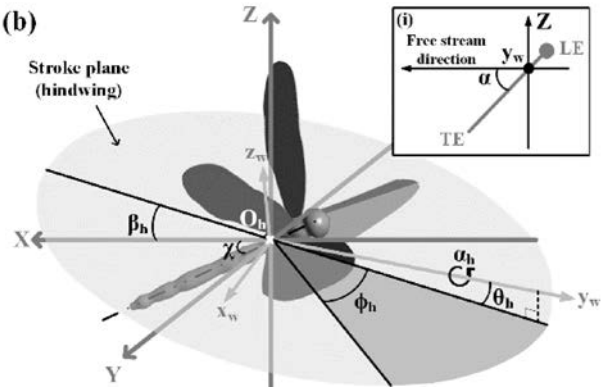

Figure 1(b). Kinematic modelling defined within the stroke plane at the global coordinate system (X, Y, Z) and the local wing-fixed coordinate system (x_w, y_w, z_w). The global coordinate system is originated at the wing root of the hindwing. χ denotes the body angle and β_h denotes the stroke plane angle of the hindwing. The y_w-axis of the local wing-fixed coordinate system is defined based on the rotation axis of the pitching motion, as the line connecting the wing tip to the wing root. The position angle ϕ and elevation angle θ are defined in the local wing-fixed coordinate system as counter-clockwise rotation about z_w-axis and counter-clockwise rotation about x_w-axis. (i) Definition of α, it is the geometric angle of attack at 60% wing length with respect to the free-stream velocity. The projection of the wing at the X-Z plane is illustrated by the grey line with solid dot showing the leading edge (LE) and TE denoting the trailing edge.

2.2 Computational fluid dynamic (CFD) modelling

In the CFD analysis, ANSYS Fluent solves the continuity and momentum equations of the incompressible fluid around the wing; whereas, in the CSM analysis, ANSYS Mechanical calculates the deformation and motion of the wing.

The overall CFD computational domain shown in Fig. 2(a) was based on the symmetrical right half of a spherical fluid enclosure with a radius of up to 15 chord lengths away from the wing root, which

was done to avoid the unstable reflection of the solution at the fluid boundary [17, 18]. The overall computational domain consisted of a near- and a far-field fluid domain.

As shown in Fig. 2(a), the overall fluid domain was meshed using tetrahedral elements to give a total of 0.2 million volume cells around the fore- and hind-wing. The near-field fluid domain was 4 chord lengths away from the wing root, and meshed such that the grid was denser near the tips and edges of the wing, and coarser towards the far-field. The grids were mapped between the near-field and the far-field boundary faces and increased with a growth rate of 1.5, so that the grid points were clustered around the wing, and gradually increased in size towards the far-field. These set-ups were done to ensure that the viscous flow at the leading edge, trailing edges and the wing tip would be captured at a higher resolution and in greater accuracy and detail. In addition, the computational time was reduced if non-uniform grids were used.

As illustrated in Fig. 2(a), the surface boundary of the fluid enclosure was divided into the velocity inlet with free stream conditions applied, and the pressure outlet with the ambient pressure conditions applied. The velocity in the X-direction was set to 1.7 m/s, and 0 m/s in the other directions, to ensure that the analysis was carried out with the dragonfly moving forward in the negative X-direction. The velocity in the X-direction was calculated from the dragonfly's experimental kinematic data [4], so that the simulated dragonfly moved in a slow forward fashion with an advance ratio, $J = U/2\Phi\omega R = 0.38$ (where U is the free stream velocity, Φ the flapping amplitude in radians, ω the flapping frequency and R the wing length), similar to Wakeling and Ellington's.

Moreover, impermeable and no-slip wall conditions were applied at the interface between the wings and the fluid. At the plane of symmetry, flow symmetry conditions were applied.

In the present CFD modelling, the unsteady incompressible Navier-Stokes equations were solved using ANSYS Fluent. The Reynolds number at which the simulations were performed can be calculated by:

$$\mathrm{Re} = \frac{U_{ref} L_{ref}}{\nu}, \qquad (1)$$

where ν is the kinematic viscosity of air (1.5×10^{-5} m^2s^{-1}); L_{ref} is the reference length of the mean chord length; and U_{ref} is the free stream air velocity (1.7 m/s). For the slow forward dragonfly flight, the mean chord lengths are 5.54 mm and 7.45 mm of the fore- and hind-wing respectively, Re is approximately between 630 and 840.

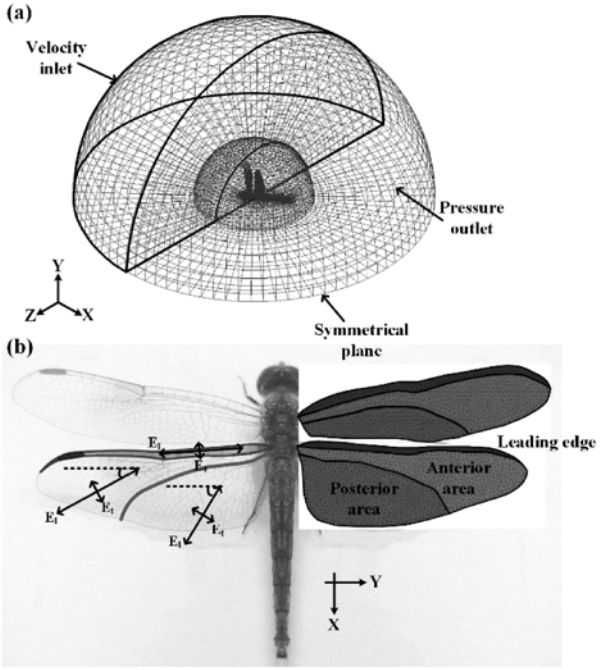

Figure 2. Computational domain, mesh and boundary conditions for the CFD model. (a) The semi-spherical computational domain consisting of the near- and far-field domains, and the applied boundary conditions. (b) CSM structural wing models of the dragonfly with their real counterpart, taken into consideration the vein distribution and anisotropy of wing material properties. El indicates the longitudinal Young's modulus, which aligns parallel to the vein directions and Et, the transverse Young's modulus, which is perpendicular to the vein directions.

The key quantities to examine are the vertical force coefficient C_V, the thrust coefficient C_T and the pressure coefficient C_p defined as follows:

$$C_V = \frac{V}{0.5\rho U_{ref}{}^2 A_{ref}}, \qquad (2)$$

and

$$C_T = \frac{T}{0.5\rho U_{ref}{}^2 A_{ref}}, \qquad (3)$$

and

$$C_p = \frac{P}{0.5\rho U_{ref}{}^2}, \qquad (4)$$

where A_{ref} is the reference area which is the wing planform area, V is vertical force, T is thrust, P is pressure and ρ is the air density.

For the solution method, the pressure-velocity coupling was accomplished via the SIMPLE algorithm with the second-order upwind spatial discretization, and a time step size of 2.5×10^{-5} s. For the convergence criteria, the residuals of

continuity and velocities had to be reduced more than three orders of magnitude in each time step.

2.3 Structural modelling of flexible dragonfly wings

Past morphological and structural studies have illustrated that the dragonfly wings are supported by veins and membranes [19-24]. The veins are clustered and thickened near the wing root but tapered in both spanwise and chordwise directions toward the wing tip and trailing edge respectively [21, 25-29]. Therefore, both the fore- and hind-wing are divided into three regions according to their relative stiffness: Leading edge, Anterior and Posterior areas.

The leading edge region were made of the foremost and thickest leading edge veins including costa, subcostal and radius [30], whereas the main area behind the leading edge was divided by the anterior median vein (MA) into anterior and posterior areas [20, 31, 32]. Usually the anterior area is relatively stiff and reinforced by a concentration of veins, and the posterior area is less supported thus more flexible. In order to account for the mass distribution as well as the different relative stiffness of each region in our modelled wing with uniform thickness, different values of material density and effective in-plane stiffness constants are assigned to each region to represent the actual wing as close as possible.

Unlike the unidirectional fibre reinforcement in the hawkmoth wings [18, 33-35], the dragonfly wing's stiffness is reinforced in the spanwise direction by allocating the chordwise cross veins between the longitudinal veins, while at the same time allowing torsion and enhancing the development of wing camber [27, 36, 37]. Therefore, the dragonfly wings were treated as fibre reinforced symmetric cross-ply composite material in the present study.

The following steps were taken to derive the appropriate material properties for the present structural dragonfly wing model:

(1) The whole wing was divided into three regions (Leading edge, Anterior and Posterior areas) of distinct flexibility according to the distribution of venation patterns.

(2) Referring to past investigations of dragonfly wings [27, 38], the Young's modulus of the vein and membrane are taken as 6 GPa and 3.7 GPa, respectively. The vein and membrane thickness is not constant over the wing. Therefore, the average thickness of each of the wing sections is used. Since the mass and bending stiffness are proportional to t_{vein} and t_{vein}^3 [39], respectively, the membrane density is modified by multiplying a membrane-to-vein thickness ratio α_m (<1) while its Young's modulus is re-defined by multiplying a coefficient of α_m^3. Hence, the equivalent Young's modulus and density of the vein and membrane at each wing region are calculated and used in the uniform thickness wing model.

(3) As the relatively rigid longitudinal veins are structurally intact and not interrupted by resilin patches, they will resist flexion along the span of the wing, while mobility in the joints where cross-veins meet the longitudinal veins allows the wing to flex along the chord [40]. The above evidence supports the uncoupling between the longitudinal and cross vein in the dragonfly wings. Thus an equivalent symmetric cross-ply composite model is adopted for the dragonfly structural wing model in the effort to represent the reality as close as possible. Detailed evaluation of the effective material properties of the symmetric cross-ply composite used in the present dragonfly model can be found in the references [41, 42].

In addition, a Poisson's ratio of 0.49 was chosen, the same as used in other studies [35, 43, 44], as varying the Poisson's ratio do not affect the results of the simulation significantly [38, 43, 45].

3 Results and Discussion

The grid sensitivity and domain size tests are conducted for the present FSI wing model to ensure the accuracy of the simulations in Sec. 3.1. The FSI solver is then validated against well-established past experiments and simulations in Sec. 3.2.

3.1 Self-consistency of the numerical solver

The verification of the self-consistency of the numerical solver was done in two steps. First, the grid sensitivity and domain size were tested in the CFD solver. Second, the grid size was further verified in the CSM solver, along the process, the material properties used in the present simulation are also validated.

To test the grid sensitivity in the CFD solver, a baseline case with the minimum grid size of 0.8 mm, which is 50 % of the boundary layer thickness at the wing trailing edge, was compared to a refined case with the minimum grid size of 0.016 mm, similar to 1 % of the boundary layer thickness at the trailing edge used by Liu and Kawachi in rigid wing CFD [46]. For simplicity and efficiency, a simple harmonic wing kinematics [35] was used at the wing

base for the single rigid dragonfly hindwing model when running the verifications.

The resultant vertical and horizontal force coefficients of the two cases differed by 1.2 % and 1.6 % respectively, confirming that the grid refinement did not significantly affect the simulation results. In consideration of the triple computational time needed to run the refined case, and the negligible differences in the computational results, the baseline setting of the grid size was adapted in the present simulations. In addition, the appropriate time step size was chosen in favour of running the dynamic remeshing process smoothly, and decided to be 2.5×10^{-5} s for the baseline case.

Furthermore, two domain sizes were tested in the CFD solver to verify its self-consistency in terms of the mesh resolution at the wing vicinity. A smaller domain with a radius of 15 times the mean chord length was compared to a larger domain with a radius of 50 times the mean chord length. The differences in the computed vertical and horizontal force coefficients between the smaller and larger domain cases were insignificant, with a value of 0.2% and 3%, respectively. Thus, the smaller domain size with a radius of 15 times the mean chord length was used in the present simulations.

After verification of the grid sensitivity and domain size in the CFD solver, we then verified the grid size in the CSM solver. The structural model of the dragonfly forewing in the CSM solver was meshed with three different minimum grid sizes, namely, 0.2 mm, 0.4 mm and 0.8 mm. These FEM models then underwent the chordwise bending tests following the setups of Combes and Daniel [33]. In their experiments, a static point load of F = 0.3 mN was applied at 70% of chord length and halfway between the wing root and tip, while the leading edge was fixed [43]. As shown in Fig. 3, the resultant deflection δ of the wing in the Z-direction at the point of force exertion is approximately the same when comparing the cases of grid size 0.2 mm and 0.4 mm (both case have a value of δ = -0.023), however, δ varies significantly between the 0.8 mm case (δ = -0.017) and the other cases. Due to the fact that the 0.4 mm case lead to a 100 % mesh mapping at the interface of the fluid and structural model, as well as adequate resolution, this grid size was used in the CSM solver.

Moreover, through the bending tests, the material properties used in the present simulations were validated against the measurements from past experiments. According to [33], the flexural stiffness EI of the insect wing can be calculated by:

$$EI = \frac{FL^3}{3\delta}, \quad (5)$$

where F is applied point force, L is the effective length from the fixed support to the point of force application, and δ is wing displacement in the Z-direction at the point of force application, namely at 70 % span or chord length.

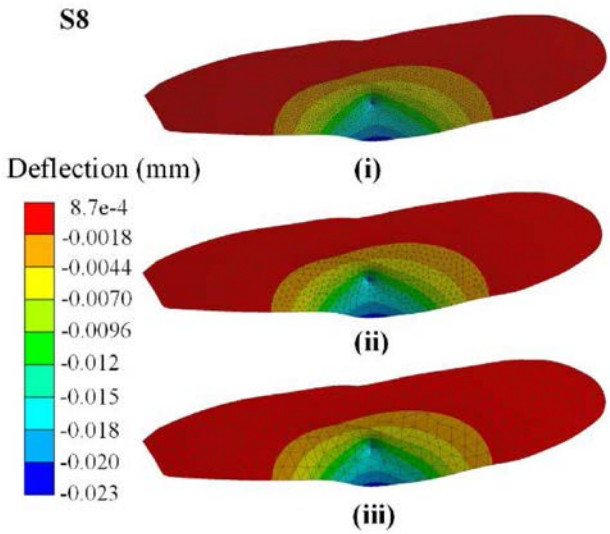

Figure 3. Flexible structural forewing model used for the grid sensitivity and bending test validation. The resultant overall wing deflections in the Z-direction are shown for the chordwise bending test, including grid sensitivity tests of (i) grid size = 0.2 mm, (ii) grid size = 0.4 mm and (iii) grid size = 0.8 mm.

For the chosen grid size of 0.4 mm, the calculated chordwise flexural stiffness is 4.1×10^{-7} Nm^2, which is in the same order of 10^{-7} as past measurements [43]. Additionally, the spanwise bending test following the same procedure as in [33] was also carried out for the grid size of 0.4 mm case to further validate the spanwise flexural stiffness with experiments. The point force was applied at a point of 70 % of wing span near the leading edge, while the wing root was fixed for spanwise bending test. The resultant point deflection δ = -0.044 gives rise to a spanwise flexural stiffness of 2.1×10^{-5} Nm^2, well within the same order of 10^{-5} as in [33].

3.2 Comparisons with past simulations

To further validate the present FSI solver, a flexible hawkmoth in hovering flight was simulated and compared to Nakata and Liu [18, 35]. In this validation test, the wing geometry, material properties and flapping kinematics were based on the investigations in [18, 35].

The hawkmoth wing model used the same outline of a real hawkmoth wing planform with

wing length, 48.3 mm and mean chord length, 18.3 mm; and a uniform thickness of 0.6 mm. To account for the variation of the wing flexibility due to different thickness and stiffness of the veins and membranes distributing across the wing, the hawkmoth wing model was divided into three regions: leading edge, forewing and hindwing, and in each region an anisotropic material was assigned accordingly. The veins of the hawkmoth wing are mainly running in the same direction in each wing region [18, 35, 43]. Thus, the longitudinal and transverse Young's modulus are calculated and assigned to each wing region, according to the respective parallel and perpendicular alignment to the vein direction. However, at the stiffer leading edge region, the material is more or less isotropic. Therefore, the same value is used for both longitudinal and transverse Young's moduli at the leading edge region.

The same simplified flapping kinematics of the hawkmoth as used by Nakata and Liu was implemented for this validation. Note that however the angle of attack α is defined as the averaged value of the measured angles of attack at the wing root and the wing tip [34, 35, 46, 47].

Figure 4 illustrates the time history of the vertical and horizontal force coefficients as compared to that of Nakata and Liu in one corresponding flapping cycle. The trends and amplitudes of the force coefficients are very similar between the two studies over most of the flapping cycle, during the main translational strokes and before stroke reversal. The main variation in the amplitudes occurs after stroke reversal, at 15 % of flapping cycle (see t_1 in Fig. 4(a)).

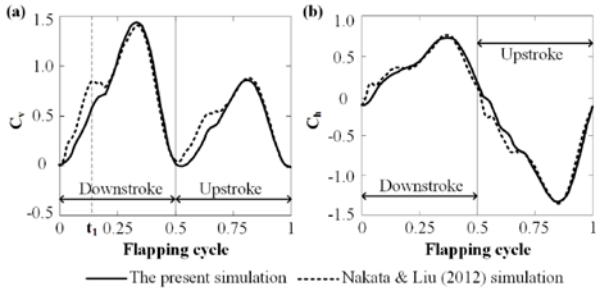

Figure 4. Comparison of our computed force coefficients with the computational results of Nakata and Liu [35] in one corresponding flapping cycle. (a) Vertical force coefficient C_v and (b) Horizontal force coefficient C_h. The vertical dash line marks the time t_1 when the main difference in magnitude occurs between the two studies.

Despite the slight differences after stroke reversal, the present FSI simulation results shown in Fig. 4 are definitely within any reasonable error margin. From the above validation with past studies, together with the solver self-consistency analysis in Sec. 3.1, we are confident that the present simulation can capture the aerodynamic forces, the flows and the interactions between the fluid and the flapping dragonfly wings with reasonable accuracy.

4 Conclusion

ANSYS Fluent, ANSYS Mechanical and the System Coupling packages from ANSYS Workbench 16.2 was used in creating the wing model, meshing, and two-way coupling of the computational fluid dynamic (CFD) solver and the finite element method (FEM) based computational structure mechanics (CSM) solver.

The whole wing was divided into three regions (Leading edge, Anterior and Posterior areas) of distinct flexibility according to the distribution of venation patterns. The equivalent Young's modulus and density of the vein and membrane at each wing region are calculated and used in the uniform thickness wing model. The uncoupling between the longitudinal and cross vein in the dragonfly wings was utilized.

Several steps of verification and validations were performed. First, a simple harmonic wing kinematics was utilized at the wing base for a single rigid dragonfly hindwing model to ensure sufficient domain size and grid resolution for the CFD. Second, the grid size for the CSM solver, along with the material properties, was verified by performing chordwise bending tests. The simulation results showed agreement with past experiments. Third, a flexible hawkmoth in hovering flight was simulated and compared to previous investigations. A number of force coefficients were evaluated over the flapping cycle and good agreement was accomplished.

The simulation framework has been rigorously proven to capture both the fluid flow and structural mechanics, including the two-way coupling, and can in the future be utilized for the development of flapping-wing micro-air vehicles with a biomimetic approach.

References:

1. C. Somps and M. Luttges, Dragonfly Flight: Novel Uses of Unsteady Separated Flows, *Science*, Vol.228, No.4705, 1985, pp. 1326-1329.
2. H. Nagai, A. Nishi, T. Fujimoto, and K. Isogai. Study on flow interaction mechanism of fore- and hindwings of dragonfly. in *Proceedings of*

the 4th International Symposium on Aero Aqua Bio-Mechanisms. 2009. Shanghai, China.
3. A.L.R. Thomas, G.K. Taylor, R.B. Srygley, R.L. Nudds, and R.J. Bomphrey, Dragonfly flight: free-flight and tethered flow viualisations reveal a diverse array of unsteady lift-generating mechanisms, controlled primarily via angle of attack, *J. Exp. Biol.*, Vol.207, 2004, pp. 4299-4323.
4. J.M. Wakeling and C.P. Ellington, Dragonfly flight. II. Velocities, accelerations and kinematics of flapping flight, *J. Exp. Biol.*, Vol.200, No.3, 1997, pp. 557-582.
5. M. Sun and J. Tang, Unsteady aerodynamic force generation by a model fruit fly wing in flapping motion, *J. Exp. Biol.*, Vol.205, 2002, pp. 55-70.
6. M. Sun and S.L. Lan, A computational study of the aerodynamic forces and power requirements of dragonfly (*Aeschna juncea*) hovering, *J. Exp. Biol.*, Vol.207, No.11, 2004, pp. 1887-1901.
7. M.J.C. Smith, Simulating moth wing aerodynamics - Towards the development of flapping-wing technology *AIAA J.*, Vol.34, No.7, 1996, pp. 1348-1355.
8. M.J.C. Smith, P. Wilkin, and M. Williams, The advantages of an unsteady panel method in modelling the aerodynamic forces on rigid flapping wings, *J. Exp. Biol.*, Vol.199, No.5, 1996, pp. 1073-1083.
9. M.J.C. Smith and S.S. Zenieh. Trajectory Control of Flapping Wings: Towards the Development of Flapping-Wing Technology. in *AIAA, NASA, and ISSMO, 6th Symposium on Multidisciplinary Analysis and Optimization*. 1996. Bellevue WA, USA: AIAA J.
10. J. Young, S.M. Walker, R.J. Bomphrey, G.K. Taylor, and A.L.R. Thomas, Details of Insect Wing Design and Deformation Enhance Aerodynamic Function and Flight Efficiency, *Science*, Vol.325, No.5947, 2009, pp. 1549-1552.
11. S.M. Walker, A.L.R. Thomas, and G.K. Taylor, Photogrammetric reconstruction of high-resolution surface topographies and deformable wing kinematics of tethered locusts and free-flying hoverflies, *J. R. Soc. Interface*, Vol.6, No.33, 2009, pp. 351-366.
12. S.M. Walker, A.L.R. Thomas, and G.K. Taylor, Deformable wing kinematics in the desert locust: how and why do camber, twist and topography vary through the stroke?, *J. R. Soc. Interface*, Vol.6, No.38, 2009, pp. 735-747.
13. S.M. Walker, A.L.R. Thomas, and G.K. Taylor, Deformable wing kinematics in free-flying hoverflies., *J. R. Soc. Interface*, Vol., 2009, pp. Published online.
14. Y.H. Chen, M. Skote, Y. Zhao, and W.M. Huang, Stiffness evaluation of the leading edge of the dragonfly wing via laser vibrometer, *Materials Letters*, Vol.97, 2013, pp. 166-168.
15. Y.H. Chen, M. Skote, Y. Zhao, and W.M. Huang, Dragonfly (Sympetrum flaveolum) flight: Kinematic measurement and modelling, *Journal of Fluids and Structures*, Vol.40, 2013, pp. 115-126.
16. Y.H. Chen and M. Skote, Study of lift enhancing mechanisms via comparison of two distinct flapping patterns in the dragonfly Sympetrum flaveolum, *Physics of Fluids*, Vol.27, No.3, 2015, pp. 033604.
17. T. Weis-Fogh, Quick estimates of flight fitness in hovering animals, including novel mechanisms for lift production, *J. Exp. Biol.*, Vol.59, 1973, pp. 169-230.
18. T. Nakata and H. Liu, Aerodynamic performance of a hovering hawkmoth with flexible wings: a computational approach, *Proceedings of the Royal Society B-Biological Sciences*, Vol.279, No.1729, 2012, pp. 722-731.
19. S. Sudo, K. Tsuyuki, and J. Tani, Wing morphology of some insects, *JSME International Journal Series C-Mechanical Systems, Machine Elements and Manufacturing*, Vol.43, No.4, 2000, pp. 895-900.
20. R.J. Wootton, Support and deformability in insect wings, *J. Zool.*, Vol.193, 1981, pp. 447-468.
21. R.J. Wootton, Functional morphology of insect wings, *Annu. Rev. Entomol.*, Vol.37, No.1, 1992, pp. 113-140.
22. R.J. Wootton, Geometry and Mechanics of Insect Hindwing Fans: A Modelling Approach, *Proc. Roy. Soc. Lond. B Biol. Sci.*, Vol.262, No.1364, 1995, pp. 181-187.
23. C.J.C. Rees, Form and function in corrugated insect wings, *Nature*, Vol.256, No.5514, 1975, pp. 200-203.
24. Y.H. Chen and M. Skote, Gliding performance of 3-D corrugated dragonfly wing with spanwise variation, *Journal of Fluids and Structures*, Vol.62, 2016, pp. 1-13.
25. M.L. May, Dragonfly Flight: Power Requirements at High Speed and Acceleration, *Journal of Experimental Biology*, Vol.158, No.1, 1991, pp. 325-342.
26. A. Vargas, R. Mittal, and H. Dong, A computational study of the aerodynamic performance of a dragonfly wing section in

gliding flight., *Bioinspiration & Biomimetics*, Vol.3, 2008, pp. 1-13.
27. A.B. Kesel, U. Philippi, and W. Nachtigall, Biomechanical Aspects of the Insect Wing: An Analysis Using the Finite Element Method., *Comput. Biol. Med.*, Vol.28, 1998, pp. 423-437.
28. M. Okamoto, K. Yasuda, and A. Azuma, Aerodynamic Characteristics of the Wings and Body of A Dragonfly, *J. Exp. Biol.*, Vol.199, 1996, pp. 281-294.
29. M. Mingallon and S. Ramaswamy. The architecture of the dragonfly wing: a study of the structural and fluid dynamic capabilities of the ansoptera's forewing. in *Proceedings of the ASME 2011 International Mechanical Engineering Congress & Exposition, IMECE2011*. 2011. November 11-17, Denver, Colorado, USA.
30. A.B. Kesel, Aerodynamic Characteristics of Dragonfly Wing Sections Compared with Technical Aerofoils, *J. Exp. Biol.*, Vol.203, 2000, pp. 3125-3135.
31. R.J. Wootton, Function, homology and terminology in insect wings, *Syst. Entomol.*, Vol.4, No.1, 1979, pp. 81-93.
32. R.J. Wootton, J. Kukalová-Peck, D.J.S. Newman, and J . Muzón, Smart engineering in the mid-carboniferous: How well could palaeozoic dragonflies fly?, *Science*, Vol.282, No.5389, 1998, pp. 749-751.
33. S.A. Combes and T.L. Daniel, Flexural stiffness in insect wings II. Spatial distribution and dynamic wing bending, *J. Exp. Biol.*, Vol.206, No.17, 2003, pp. 2989-2997.
34. H. Liu, C.P. Ellington, K. Kawachi, C. Van Den Berg, and A.P. Willmott, A computational fluid dynamic study of hawkmoth hovering, *J. Exp. Biol.*, Vol.201, No.4, 1998, pp. 461-477.
35. T. Nakata and H. Liu, A fluid–structure interaction model of insect flight with flexible wings, *Journal of Computational Physics*, Vol.231, No.4, 2012, pp. 1822-1847.
36. A.R. Ennos, Mechanical Behaviour in Torsion of Insect Wings, Blades of Grass and other Cambered Structures, *Proc. Roy. Soc. Lond. B Biol. Sci.*, Vol.259, No.1354, 1995, pp. 15-18.
37. R.A. Norberg, The Pterostigma of Insect Wings an Inertial Regulator of Wing Pitch, *J. Comp. Physiol.*, Vol.81, 1972, pp. 9-22.
38. S.R. Jongerius and D. Lentink, Structural Analysis of a Dragonfly Wing, *Experimental Mechanics*, Vol.50, No.9, 2010, pp. 1323-1334.
39. S. Timoshenko and S. Woinowsky-Krieger, *Theory of Plates and Shells*. 1959, New York: McGraw-Hill Book Co., Inc.
40. S. Donoughe, J.D. Crall, R.A. Merz, and S.A. Combes, Resilin in dragonfly and damselfly wings and its implications for wing flexibility, *Journal of Morphology*, Vol.272, No.12, 2011, pp. 1409-1421.
41. R.M. Jones, *Mechanics of composite materials*. 2nd ed. 1999: Philadelphia, PA : Taylor & Francis, c1999.
42. A.K. Kaw, *Macromechanical Analysis of Laminates*, in *Mechanics of Composite Materials, Second Edition*. 2005, CRC Press. p. 315-367.
43. S.A. Combes and T.L. Daniel, Flexural stiffness in insect wings I. Scaling and the influence of wing venation, *J. Exp. Biol.*, Vol.206, No.17, 2003, pp. 2979-2987.
44. T. Nakata, Aerodynamic performance of flapping flexible wing in insect flight, *Comp. Biochem. Physiol. Mol. Integr. Physiol.*, Vol.153, No.2, Supplement 1, 2009, pp. S50-S52.
45. D.J.S. Newman and R.J. Wootton, An Approach to the Mechanics of Pleating in Dragonfly Wings, *J. Exp. Biol.*, Vol.125, No.1, 1986, pp. 361-372.
46. H. Liu and K. Kawachi, A Numerical Study of Insect Flight, *J. Comput. Phys.*, Vol.146, No.1, 1998, pp. 124-156.
47. A.P. Willmott and C.P. Ellington, The mechanics of flight in the hawkmoth Manduca sexta. I. Kinematics of hovering and forward flight, *The Journal of Experimental Biology*, Vol.200, No.21, 1997, pp. 2705-2722.
48. S. Ho, H. Nassef, N. Pornsinsirirak, Y.-C. Tai and C.-M. Ho, Unsteady aerodynamics and flow control for flapping wing flyers, *Progress in Aerospace Sciences* Vol.39, 2003, pp. 635–681.